

# Nanoscale Heterogeneity of the Molecular Structure of Individual hIAPP Amyloid Fibrils Revealed with Tip-Enhanced Raman Spectroscopy

Corianne C. vandenAkker, Tanja Deckert-Gaudig, Michael Schleegeer, Krassimir P. Velikov, Volker Deckert,\* Mischa Bonn, and Gijsje H. Koenderink\*

*Type 2 diabetes mellitus is characterized by the pathological deposition of fibrillized protein, known as amyloids. It is thought that oligomers and/or amyloid fibrils formed from human islet amyloid polypeptide (hIAPP or amylin) cause cell death by membrane damage. The molecular structure of hIAPP amyloid fibrils is dominated by  $\beta$ -sheet structure, as probed with conventional infrared and Raman vibrational spectroscopy. However, with these techniques it is not possible to distinguish between the core and the surface structure of the fibrils. Since the fibril surface crucially affects amyloid toxicity, it is essential to know its structure. Here the surface molecular structure and amino acid residue composition of hIAPP fibrils are specifically probed with nanoscale resolution using tip-enhanced Raman spectroscopy (TERS). The fibril surface mainly contains unordered or  $\alpha$ -helical structures, in contrast to the  $\beta$ -sheet-rich core. This experimentally validates recent models of hIAPP amyloids based on NMR measurements. Spatial mapping of the surface structure reveals a highly heterogeneous surface structure. Finally, TERS can probe fibrils formed on a lipid interface, which is more representative of amyloids in vivo.*

## 1. Introduction

Amyloid fibrils are self-assembled,  $\beta$ -sheet-rich aggregates formed by a large class of peptides and proteins. Many protein-misfolding diseases, such as type 2 diabetes mellitus and Alzheimer's disease, are characterized by the pathological deposition of amyloid fibrils.<sup>[1]</sup> These fibrils are generally a

few nanometers in diameter and up to several micrometers in length. Structurally, amyloid fibrils are defined by a universal cross- $\beta$  core structure that is stabilized by hydrogen bonds, causing a remarkably high mechanical rigidity.<sup>[2,3]</sup> However, amyloid fibrils are highly polymorphic. Depending on assembly conditions such as pH and ionic strength, different

Dr. C. C. vandenAkker, Prof. G. H. Koenderink  
FOM Institute AMOLF  
Science Park 104, 1098 XG Amsterdam, The Netherlands  
E-mail: g.koenderink@amolf.nl

Dr. T. Deckert-Gaudig, Prof. V. Deckert  
Leibniz Institute of Photonic Technology  
Albert-Einstein-Straße 9, 07745 Jena, Germany  
E-mail: volker.deckert@ipht-jena.de

Dr. M. Schleegeer, Prof. M. Bonn  
Department of Molecular Spectroscopy  
Max Planck Institute for Polymer Research  
Ackermannweg 10, 55128 Mainz, Germany

DOI: 10.1002/sml.201500562

Dr. K. P. Velikov  
Soft Condensed Matter  
Debye Institute for Nanomaterials Science  
Department of Physics and Astronomy  
Utrecht University  
Princetonplein 5, 3584 CC Utrecht, The Netherlands

Dr. K. P. Velikov  
Unilever Research Labs  
NL-3133 AT Vlaardingen, The Netherlands  
Prof. V. Deckert  
Institute for Physical Chemistry and Abbe Center of Photonics  
University of Jena  
Helmholtzweg 4, 07743 Jena, Germany



fibril morphologies such as twisted fibrils or ribbons can be formed.<sup>[4,5]</sup> Furthermore, under any given set of conditions, multiple polymorphic forms are typically observed.<sup>[6–8]</sup>

Human islet amyloid polypeptide (hIAPP), also called amylin, forms amyloid fibrils in the pancreas of patients suffering from type 2 diabetes mellitus and causes death of  $\beta$ -cells.<sup>[9,10]</sup> The hIAPP monomer is co-secreted with insulin by the  $\beta$ -cells in the islets of Langerhans and is thought to play a role in the regulation of glucose homeostasis.<sup>[11]</sup> Interactions of hIAPP with lipid membranes are thought to play an important role in the pathogenesis of diabetes.<sup>[12,13]</sup> Both oligomers<sup>[14,15]</sup> and fibrils<sup>[16,17]</sup> may be cytotoxic, via membrane binding and disruption of membrane integrity. On supported lipid bilayers, hIAPP has been shown to cause extensive membrane remodeling during amyloid formation.<sup>[12,18]</sup> Furthermore, membranes are thought to catalyze hIAPP oligomer formation.<sup>[13]</sup> It has been shown that negatively charged lipids can dramatically accelerate amyloid fibril formation of hIAPP as well as various other peptides.<sup>[19,20]</sup> Upon membrane binding, hIAPP monomers adopt an intermediate conformation with part of the residues incorporated into an  $\alpha$ -helix.<sup>[20,21]</sup> Subsequently, amyloid fibrils with  $\beta$ -sheet structures are formed.<sup>[21,22]</sup>

While the kinetics of hIAPP fibrillogenesis, both in bulk solution and at lipid interfaces, have been studied extensively,<sup>[8,19,23,24]</sup> structural characterization of hIAPP amyloid fibrils is still challenging. The use of X-ray crystallography and solution NMR is limited due to the insolubility and noncrystallinity of amyloid fibrils. Recently, several models of hIAPP protofibrils have been suggested based on solid-state NMR and X-ray techniques.<sup>[25–27]</sup> However, the polymorphic nature of hIAPP amyloids results in significant differences between models. Vibrational spectroscopy measurements have suggested that the molecular structure of hIAPP amyloids is dominated by  $\beta$ -sheets,<sup>[21,22,28]</sup> while nonaggregated hIAPP is mainly unstructured.<sup>[29]</sup> However, conventional infrared and Raman vibrational spectroscopy provides an ensemble measurement and therefore averages out the distinct structures of different polymorphic fibril types.<sup>[30–32]</sup> Moreover, it is not possible to distinguish between the structure of the core and the surface of the fibrils. It is important to know the surface structure, since this determines interactions of fibrils with each other and with cell membranes. Moreover, the fibril surface can potentially exert a cytotoxic effect.<sup>[33]</sup>

It was recently demonstrated that information on the structural heterogeneity as well as the surface structure of amyloid fibrils can be obtained using tip-enhanced Raman spectroscopy (TERS). In TERS, an atomic force microscope (AFM) with a metallized tip is coupled to a Raman spectrometer. Plasmonic effects at the tip apex upon laser irradiation result in a strong local Raman scattering enhancement by a factor of  $10^6$ .<sup>[34–37]</sup> The lateral spatial resolution is dependent on the dimension and shape of the tip and can reach values below 3 nm for biomolecules measured under ambient conditions.<sup>[38–40]</sup> TERS can therefore be used to map the structure of individual amyloid fibrils with nanometer resolution, as demonstrated in studies of insulin fibril surfaces<sup>[40–42]</sup> and nanotapes formed from  $\beta$ -amyloid(1–40) peptide fragments.<sup>[43]</sup> This high spatial resolution is a unique advantage

of TERS over NMR and Fourier transform IR (FT-IR) spectroscopy. Nano-FT-IR would provide high resolution too, but this technique is just emerging.<sup>[44]</sup>

Here we use TERS to investigate the surface structure of hIAPP amyloid fibrils formed in bulk solution at two different pH levels. In vitro studies on amyloids often employ an acidic solution pH to promote amyloid fibril formation.<sup>[45]</sup> Also it is known that certain peptides form amyloids in vivo at low pH values,<sup>[46]</sup> whereas for other peptides a low pH inhibits amyloid formation and membrane damage.<sup>[47]</sup> This raises the question whether fibrils formed at acidic solution pH share the same structure with fibrils formed at neutral pH levels. We compare fibrils formed in bulk solution and fibrils formed at a lipid interface composed of 1,2-dihexadecanoyl-sn-glycero-3-phospho-(1'-rac-glycerol) (DPPG). We show that TERS can map the secondary structure and the distribution of amino acid residues with nanometer lateral resolution. By comparing the surface molecular structure with the overall structure of hIAPP amyloid fibrils measured using bulk spectroscopy, we demonstrate that TERS probes primarily the fibril surface. While the fibril core is predominantly composed of  $\beta$ -sheets, the surface is heterogeneous and contains mainly unordered or  $\alpha$ -helical structures. For fibrils formed at acidic conditions, the  $\beta$ -sheet content was higher than for fibrils formed at neutral conditions. Fibrils formed on a lipid interface had a similar structure as fibrils formed in bulk.

## 2. Results and Discussion

hIAPP amyloid fibrils were prepared in bulk solution at pH = 2.0 and pH = 7.8 (both below the isoelectric point of hIAPP at 8.8)<sup>[48]</sup> and imaged using AFM and scanning transmission electron microscopy (STEM) (**Figure 1a** and **Figure S1** and **S2**, Supporting Information). Fibrils at both pH values had lengths of up to hundreds of nm and diameters between 5 and 15 nm measured based on the height determined with AFM using a silicon AFM tip. A subpopulation of fibrils with lengths up to several micrometers was also observed with STEM; however, all TERS measurements were performed on shorter fibrils.

hIAPP amyloid fibrils were deposited on glass slides, dried in air, and probed by TERS using an instrument described previously.<sup>[40,49]</sup> The inset of **Figure 1a** shows an example of a single hIAPP amyloid fibril formed at pH = 2.0, which was imaged using a standard AFM tip modified for TERS measurements. As a result of the silver particle attached to the AFM tip, the AFM image has a limited spatial resolution. However, the dimensions of the fibril are still clearly visible. Perpendicular to the fibril axis, 100 Raman spectra were measured in 0.5 nm steps along a single line, at the position indicated in white. To exclude possible effects caused by contamination of the AFM tip, a reference spectrum was recorded on the glass substrate after each grid or line measurement (**Figure S3**, Supporting Information). To determine the local peptide molecular structure, the amide I region ( $1630\text{--}1680\text{ cm}^{-1}$ ) of all 100 spectra was analyzed (**Figure 1b**). Protein secondary structures were assigned as  $\beta$ -sheet if the maximum of the band in the amide I region

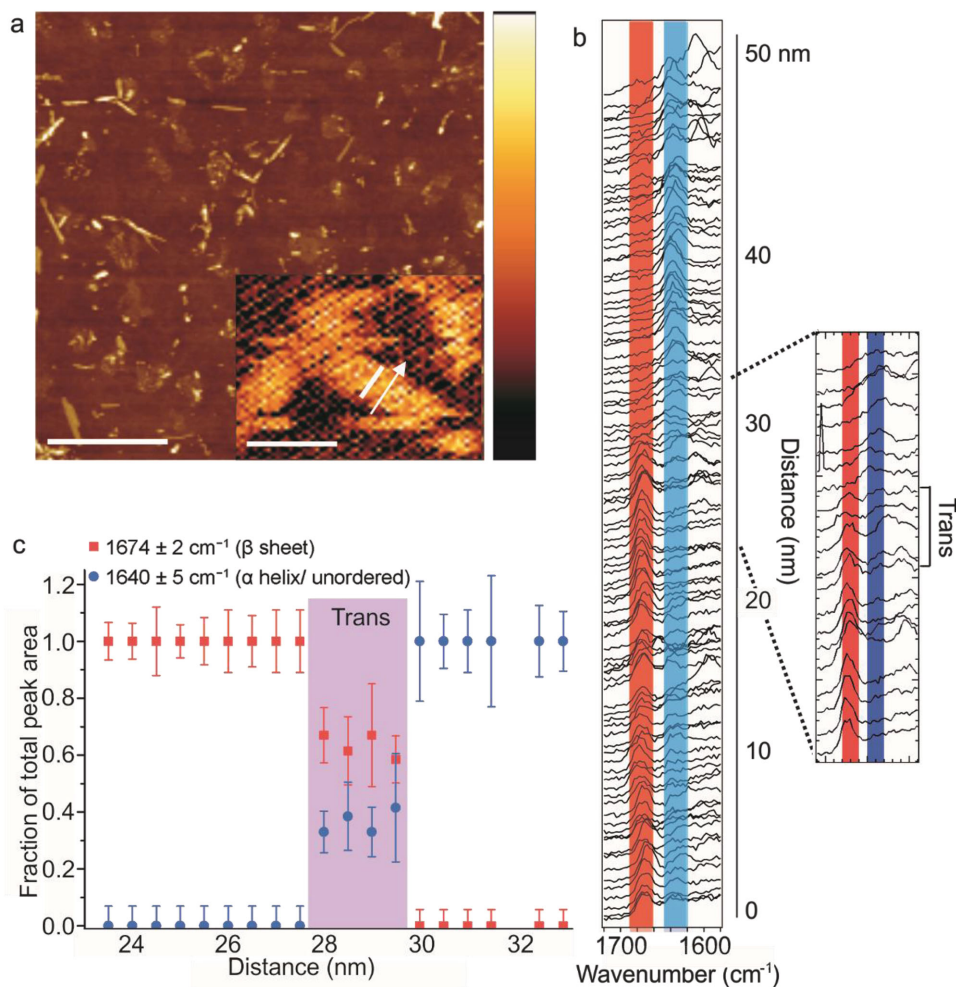


**Figure 1.** a) AFM image of hIAPP fibrils formed at pH = 2.0. Scale bar is 1  $\mu\text{m}$  and height bar is 20 nm. Inset: AFM image obtained by scanning with a TERS AFM tip. White line represents positions of the 100 TERS measurements that were recorded with 0.5 nm intervals along a line perpendicular to the fibril axis. Scale bar is 100 nm, the height bar shown in (a) represents 13.6 nm for the inset. b) Amide I region of the spectra. Red indicates band position for  $\beta$ -sheets and blue indicates for unordered or  $\alpha$ -helical structure. Right: enlarged transition region. Spectra showing mixed structures are indicated (“trans”). c) Relative secondary structure content in terms of  $\beta$ -sheets (red squares) and unordered or  $\alpha$ -helical structure (blue circles) for spectra in the transition region (spectra numbers 45–65). The distance on the x-axis corresponds to the distance from the first measurement point in Figure 1a.

was at a wavenumber between 1660 and 1680  $\text{cm}^{-1}$  and as unordered or  $\alpha$ -helical for wavenumbers between 1630 and 1655  $\text{cm}^{-1}$  (Table S1, Supporting Information).<sup>[40,41,49–51]</sup> Some spectra exhibited a broad band that encompassed both regions or they showed two distinct peaks. These spectra were allocated in a third group and considered as mixtures of  $\beta$ -sheet and unordered or  $\alpha$ -helical structures.<sup>[40]</sup> The TERS spectra measured along a line perpendicular to the fibril axis clearly show a very distinct and abrupt transition from  $\beta$ -sheet to unordered or  $\alpha$ -helical structure. One side of the fibril shows predominantly  $\beta$ -sheet structure. Approximately at the center of the fibril, a transition region of four spectra shows both  $\beta$ -sheet and unordered or  $\alpha$ -helical structure. The other side of the fibril is dominated by unordered or  $\alpha$ -helical structure. For a more detailed analysis, 20 spectra in the transition region were baseline-corrected and fitted with two Gaussian peaks. The relative peak intensities associated with the secondary structure content was inferred and plotted as a function of the distance across the fibril (Figure 1c). This

shows clearly the transition from only  $\beta$ -sheet to only unordered or  $\alpha$ -helical spectral intensity within a very small transition region (0.5 nm between points). Furthermore, it shows that the structure of this amyloid fibril is not homogeneous, but that different molecular structures are present on the fibril surface. The transition could indicate a twist of the amyloid fibril, as was speculated previously in case of insulin amyloid fibrils.<sup>[40]</sup> Another possibility is that the surface of the amyloid fibril contains clusters of a certain structure.

Not all amyloid fibrils showed such clear domains of homogeneous structure with sharp transitions in between. **Figure 2a,b** shows a topography image and a grid of  $2 \times 60$  measurement points obtained in steps of 0.5 nm measured on another hIAPP amyloid fibril formed at pH = 2.0. Four spectra with different amide I bands are shown to give an example of our analysis (Figure S3, Supporting Information). This fibril has a heterogeneous molecular structure at the surface, dominated by unordered or  $\alpha$ -helical structure, though also  $\beta$ -sheet and mixed structures are observed. For comparison,

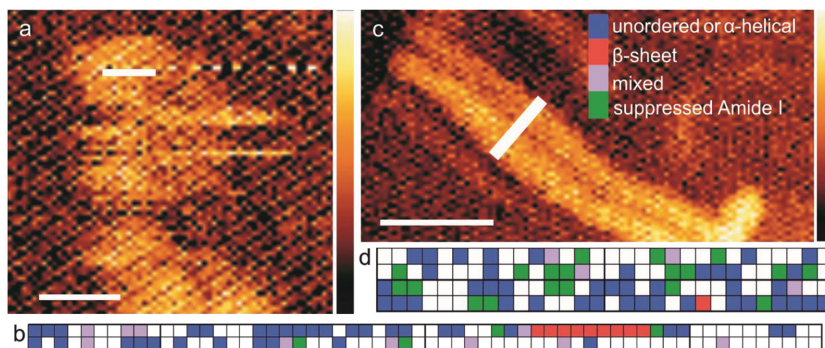


**Figure 2.** Images and structural maps of hIAPP amyloid fibrils formed at a,b) pH = 2.0 or c,d) pH = 7.8. White rectangles in the AFM topographies indicate the position of the measurements, recorded at positions spaced b) 0.5 nm or d) 2 nm apart. Colors in the map encode the local structure as judged from the amide I region. Blue: unordered or  $\alpha$ -helical structure; red:  $\beta$ -sheet; purple: mixed; and green: suppressed amide I peak. White: no spectral information was obtained, due to a loss of feedback. Scale bars are 50 nm, height bars are a) 13.3 nm and c) 14.9 nm.

Figure 2c,d shows an image and a grid of a hIAPP amyloid fibril formed at pH = 7.8. Spectra were measured in steps of 2 nm to analyze a large area of the fibril. Similar to the pH = 2.0 fibril, this fibril also predominantly contains unordered or  $\alpha$ -helical structures. Only a few spectra show  $\beta$ -sheet or mixed structures. Suppressed amide I bands are observed for 16% of the spectra, consistent with earlier TERS measurements on amyloid fibrils prepared from insulin.<sup>[49]</sup>

It has been suggested that TERS probes mainly the surface of amyloid fibrils.<sup>[40]</sup> However, in case of nanotapes formed from the Alzheimer's disease related A $\beta$ (16–22) peptide, bulk spectroscopy showed similar spectra as TERS.<sup>[52]</sup> A depth range of the evanescent field between 10 and 15 nm has been concluded in AFM-TERS,<sup>[36,53]</sup> and it has been estimated that the evanescent field decays very rapidly, by two orders

of magnitude within the first 10 nm.<sup>[54]</sup> To get a better understanding of the axial ( $z$ -) resolution obtained by TERS on hIAPP amyloid fibrils, we compared TERS measurements with attenuated total reflection FT-IR (ATR/FT-IR) spectroscopy measurements. For ATR/FT-IR measurements, a drop of amyloid fibril suspension was dried on a diamond window and IR absorption spectra were measured (Figure S4, Supporting Information). The amide I region was fitted and showed only  $\beta$ -sheet structure for both the amyloid fibrils formed at pH = 2.0 and pH = 7.8 (Tables S2 and S3, Supporting Information). This is in agreement with previous bulk spectroscopy measurements of hIAPP amyloid fibrils.<sup>[21,28]</sup> For comparison, we analyzed all TERS spectra with active amide I bands. This analysis represents an

average of six datasets for hIAPP amyloid fibrils formed at pH = 2.0 on two different fibrils and seven datasets on three fibrils for hIAPP amyloid fibrils formed at pH = 7.8. The same tip was used for all measurements on fibrils formed at one pH value. In total more than 250 spectra per condition were collected. For pH = 2.0 fibrils, amide I bands were absent in 44 out of 323 spectra (15%) and in pH = 7.8 fibrils in 61 out of 265 spectra (23%). This phenomenon is frequently observed in TERS and surface-enhanced Raman spectroscopy (SERS) experiments and is currently under investigation.<sup>[49,55]</sup>

Each spectrum was analyzed for  $\beta$ -sheet, unordered or  $\alpha$ -helical, or mixed structure contributions. For amyloid fibrils formed at pH = 2.0, more than 49% of the spectra showed only unordered or  $\alpha$ -helical structure (Figure 3a and Tables S4 and S5, Supporting Information). For 36% of the spectra,

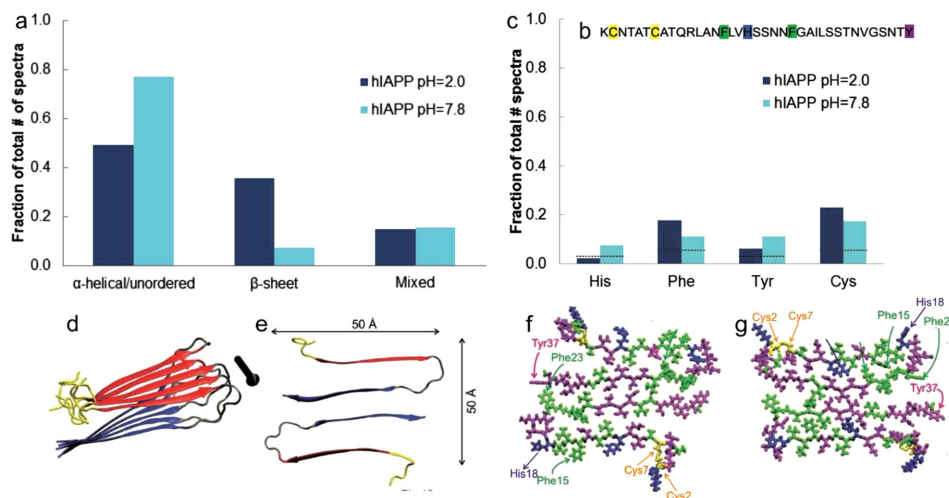


**Figure 3.** a) Molecular structure observed with TERS for hIAPP amyloid fibrils formed at pH = 2.0 (dark blue) or pH = 7.8 (light blue) averaged over datasets of more than 250 spectra with active amide I bands per condition. b) Sequence of hIAPP monomer. c) Percentage of the total number of spectra showing amino acid residues measured with TERS on hIAPP fibrils formed at pH = 2.0 or pH = 7.8. Dashed lines indicate the percentage expected based on the peptide sequence of hIAPP. d) Ribbon representation of one cross- $\beta$ -molecular layer, with N- and C-terminal  $\beta$ -strand segments in red and blue, respectively. The black arrow indicates the fibril axis. e) Cross-sectional view of two hIAPP molecules in the protofibril. f,g) All-atom representations of two possible models, with hydrophobic residues in green, polar residues in magenta, positively charged residues in blue, and disulfide-linked cysteine residues in yellow. Figure 3d–g is reproduced with permission from Luca et al.,<sup>[25]</sup> Biochemistry, ACS Publications.

only  $\beta$ -sheet was observed. The remaining spectra (15%) showed bands for both structures. For amyloid fibrils formed at pH = 7.8, the percentage of  $\beta$ -sheet is much lower: 7% of the spectra showed only  $\beta$ -sheet structure, while more than 77% showed only unordered or  $\alpha$ -helical structure and 16% showed mixed structures (Tables S4 and S6, Supporting Information).

The TERS result is clearly different from the result of bulk vibrational spectroscopy, which showed purely  $\beta$ -sheet structure for both amyloid fibrils formed under acidic and neutral conditions. These data indicate that TERS probes indeed mainly the surface structure of the amyloid fibrils. The surface of the hIAPP amyloid fibrils is heterogeneous and contains mostly unordered or  $\alpha$ -helical structures (49% or 77% for fibrils formed at respectively pH = 2.0 or pH = 7.8), while the core is composed of  $\beta$ -sheets. The fact that we observe higher  $\beta$ -sheet contents for fibrils formed at pH = 2.0 (36% vs 7% for amyloid fibrils formed at pH = 7.8) with TERS, could be related to differences in morphology of the fibrils formed under acidic conditions. Apparently more of the  $\beta$ -sheet-rich core of the fibrils is probed with TERS, while for amyloid fibrils formed at pH = 7.8 the  $\beta$ -sheet core is out of reach for the signal-enhancing field at the tip apex.

Using TERS, it is not only possible to determine the local molecular structure of amyloid fibrils but also specific amino acid residues. hIAPP is a 37-amino acid long peptide (Figure 3b), containing four different amino acid residues that can be unambiguously distinguished by their characteristic Raman bands: histidine (His), phenylalanine (Phe), tyrosine (Tyr), and cysteine (Cys)<sup>40</sup> (Table S1, Supporting Information). In combination with the known sequence of hIAPP, this analysis can provide insight in the folding of the monomers inside the fibrils. We calculated from the large datasets of all spectra the percentage of spectra showing peaks related to specific amino acid residues (Figure 3c). Dashed lines indicate the expected percentage based on the known amino acid sequence of hIAPP (1 out of 37 for His and Tyr, 2 out of 37 for Phe and Cys). His was observed in 2% of all spectra for amyloid fibrils formed at pH = 2.0, close to the expected percentage of 2.7%. In fibrils formed at pH = 7.8, the percentage of spectra showing His was approximately four times higher: 8%. Also Phe was observed much more frequently than expected statistically. This indicates that Phe is preferentially present on the surface of the amyloid fibrils, rather than in the core. Phe was detected more often on fibrils formed at pH = 2.0 and at pH = 7.8: respectively in 18% and 11% of all spectra. The same holds for Cys, which was observed in respectively 23% and 17% of all spectra for fibrils formed at pH = 2.0 and pH = 7.8. Tyr was observed in 6% of the spectra for amyloid fibrils formed at pH = 2.0, close to the expected percentage. For fibrils formed at pH = 7.8, Tyr was observed in 11% of the spectra, which is interesting since the only Tyr residue in a hIAPP peptide is found at its C-terminus. Therefore, this result indicates that fibrils formed under neutral conditions are folded in such a way that Tyr is preferentially present at the fibril surface. In contrast, in the fibrils formed under acidic conditions, Tyr appears to be masked by other amino acids. This is consistent with the higher  $\beta$ -sheet content for fibrils formed at pH = 2.0 compared to fibrils formed at

pH = 7.8 measured with TERS. Previous TERS experiments with insulin amyloids indicated that the probability of finding Phe in a  $\beta$ -sheet area is more than 12 times higher than that in an unstructured or  $\alpha$ -helical protein area.<sup>[40]</sup> This result was based on a dataset of 61 spectra. In our datasets for hIAPP fibrils, with more than 250 spectra with active amide I bands per condition, we did not observe clear indications of such preferences for any amino acids when we compared fibrils formed at different pH values (Figure S5, Supporting Information).

Besides the vibrational markers for peptide molecular structure and specific amino acids, also bands for carbonyl (C=O), imino (NH<sub>2</sub><sup>+</sup>), and amino (NH<sub>3</sub><sup>+</sup>) groups can be readily identified in TERS spectra. The presence of a peak between 1680 and 1705 cm<sup>-1</sup> or 1400 cm<sup>-1</sup> was assigned to carbonyl groups and at 1080 cm<sup>-1</sup> or 1144 cm<sup>-1</sup> to imino and amino groups.<sup>[40,41,50]</sup> There could be a small overlap between carbonyl bands and the  $\beta$ -sheet band in the amide I region, but we expect this will be a minor effect.<sup>[40,49]</sup> We observed nearly the same occurrence of carbonyl groups and imino/amino groups on amyloid fibrils formed at pH = 2.0, in respectively 5% and 7% of the spectra. For fibrils formed at pH = 7.8, the percentages are approximately a factor of two higher: 12% for carbonyl and 11% for imino/amino groups. We do not know the origin of this difference.

To interpret the TERS results concerning hIAPP folding inside the fibrils, we compared our results to existing structural models. Luca and coworkers proposed different structural models with small variations for hIAPP protofilaments formed at pH = 7.4 with a striated ribbon morphology (Figure 3d,e), based on solid-state NMR measurements and transmission electron microscopy (TEM) imaging.<sup>[25]</sup> These models are based on four layers of parallel  $\beta$ -sheets, formed by two hIAPP molecules. The dimensions of the protofilaments were  $\approx 6 \times 4$  nm, comparable to the dimensions of the fibrils we observe. In the two models shown, Phe and Cys residues are mainly present at the surface of the fibril, consistent with our TERS results (Figure 3f,g). In the model in Figure 3f, the Tyr residues in both hIAPP molecules are exposed at the surface. In contrast, in the model in Figure 3g one of the Tyr residues is shielded by other amino acids. This could explain the difference in Tyr residue abundance observed with TERS in amyloid fibrils formed at pH = 2.0 and pH = 7.8. Another fibril structure model was derived from electron paramagnetic resonance, electron microscopy and computer modeling by Bedrood et al.<sup>[27]</sup> They observed hIAPP fibrils with a left-handed twisted morphology. Also their model is based on layers of parallel  $\beta$ -sheets, formed by the regions of residues 12–19 and 31–36. These regions are smaller than in the model of Luca et al., where residues 8–17 and 28–37 form the two  $\beta$ -sheets. In both models, the residues at the N-terminus are unstructured. The fact that we observed unordered or  $\alpha$ -helical structures on the fibril surface is consistent with the predictions of the models of unstructured loops at the fibril surface.

It is generally assumed that hIAPP fibrils in vivo do not form in bulk solution but at the plasma membrane.<sup>[19,23]</sup> Membrane-binding could affect the morphology and molecular structure of amyloid fibrils. To investigate the influence of

lipid membranes on the molecular structure of hIAPP amyloid fibrils, we performed TERS measurements on amyloids formed on a simple model membrane. The hIAPP monomer solution was diluted to a concentration of  $1 \times 10^{-6}$  M in water in a trough. As a model membrane, a monolayer of the anionic lipid DPPG was formed at the air–water interface. The surface pressure was  $\approx 30$  mN m $^{-1}$ . It has been shown before that hIAPP amyloids will form at the lipid monolayer under these conditions (Figure 4a).<sup>[21,22]</sup> When the interfacial layer was transferred to a glass substrate, we indeed observed amyloid fibrils. The fibrils have diameters in the range of 3–10 nm and are up to 300 nm in length. We obtained four TERS data-sets on three fibrils with the same tip. A total of 287 spectra were recorded, of which 149 displayed suppressed amide I bands (Table S7, Supporting Information). The percentage of suppressed amide I bands (52%) is much higher than for fibrils formed in bulk at pH = 7.8 (23%)—this difference can be at least partly explained by shielding of the protein signal by the lipids. Lipid signals are apparent in at least 13% of the spectra. We compared the secondary structure on the surface of these fibrils to that of fibrils formed at pH = 7.8 in bulk. Unordered or  $\alpha$ -helical structure was observed in 68% of all spectra with an amide I band, slightly less than for amyloid fibrils formed in bulk at pH = 7.8 (77%). In 11% of the spectra only  $\beta$ -sheet was observed, while 21% of the spectra showed both unordered or  $\alpha$ -helical and  $\beta$ -sheet structure. We therefore conclude that the molecular surface structure of the fibrils formed at the lipid interface is not significantly different from fibrils formed in bulk. Nevertheless, our data do indicate subtle differences in the occurrence of amino acids at the surface of amyloid fibrils formed in bulk and at the lipid interface. His and Cys are observed more frequently in fibrils formed at the lipid interface, while Phe and Tyr are detected less frequently (Table S4, Supporting Information). Besides analysis of the local molecular structure and the amino acid residues, we also observed Raman bands characteristic of lipids on the fibrils. Bands at 1720–1750 cm $^{-1}$  can be assigned to the ester group of lipids.<sup>[56,57]</sup> Further marker bands for lipids are the bands at 1075–1090 cm $^{-1}$  and 830–840 cm $^{-1}$ , which can be assigned to PO $_2$  groups.<sup>[51,56–58]</sup> Because the band at 1085–1090 cm $^{-1}$  does not overlap with protein bands, it is a reliable indicator of lipids. Since the band at 830–840 cm $^{-1}$  is likely to interfere with the Tyr ring breathing mode, we did not use it for lipid detection.

Figure 4b shows an AFM image of an amyloid fibril formed at a lipid interface. TERS measurements were performed along the black line in 1 nm steps. Figure 4c shows 7 of the 100 spectra that were measured at the position of the black rectangle, selected to show the diversity on the amyloid fibril surface. Spectra 1 and 2 show marker bands for lipids (PO $_2$ ), but no band in the amide I region. In spectrum 3 no amide I band, nor marker bands for lipids are measured. Spectra 4 and 5 contain unordered or  $\alpha$ -helical structure bands and the peaks between 1085 and 1090 cm $^{-1}$  are assigned to lipids. Spectra 6 and 7 have peaks both for  $\beta$ -sheet and for unordered or  $\alpha$ -helical structure. Furthermore, in spectrum 6 also a lipid marker band is observed. We conclude that the surface of the fibril is highly heterogeneous in molecular structure and is partly covered by lipid

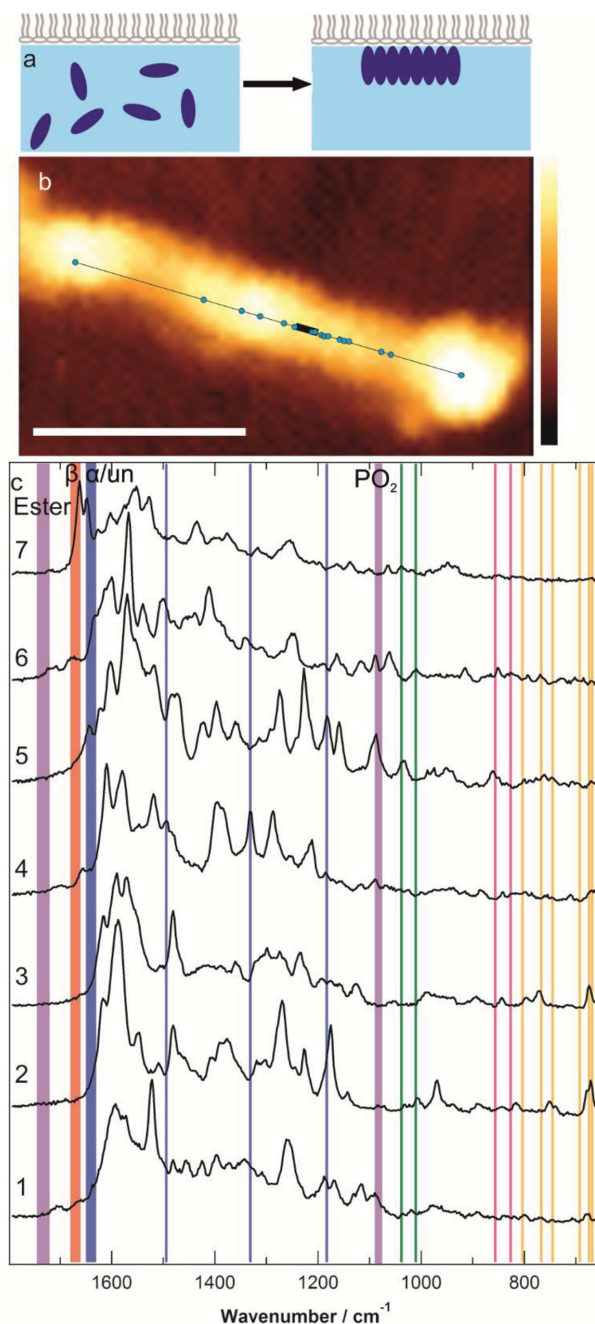


**Figure 4.** a) Schematic of the formation of amyloid fibrils at the lipid interface. Left: hIAPP monomer in solution with a lipid monolayer at the air–water interface. Right: hIAPP amyloid fibrils formed at the lipid interface. b) AFM image of an amyloid fibril formed at a lipid interface. Black line indicates the entire line where TERS spectra were measured, the black box refers to the positions of the spectra shown in (c). Blue circles indicate the positions of spectra showing lipids. Scale bar is 50 nm and height bar is 6.4 nm. c) Spectra measured at 1 nm steps on the amyloid fibril showing band for: 1,2) lipids. 3) No lipids and no amide I. 4,5) Unordered or  $\alpha$ -helical structure and lipids. 6) Mixed structure and lipids. 7) Mixed structure. Bands—red:  $\beta$ -sheet; blue: unordered or  $\alpha$ -helix; and purple: lipids. Lines—blue: His; green: Phe; pink: Tyr; and orange: Cys.

molecules. This is in agreement with other studies showing interactions between mature amyloid fibrils and lipid molecules, for hIAPP as well as for other peptides.<sup>[12,59]</sup> In general,

the relation between amyloid fibril structure and the pathogenesis of amyloidogenic diseases is still poorly understood. There is strong evidence that the structure affects membrane-binding, which in turn is connected to cellular cytotoxicity. In the context of diabetes, circular dichroism studies have shown that hIAPP binds membranes in an  $\alpha$ -helical conformation, and that a conversion to  $\beta$ -sheet structures occurs upon oligomerization.<sup>[13]</sup> Although the precise mechanism of membrane permeabilization of hIAPP is still unknown, there are indications that the  $\alpha$ -helical conformation of hIAPP may have membrane-disrupting properties.<sup>[13]</sup> Thus, the surface structure of the hIAPP amyloid fibrils is likely to influence the pathogenesis of diabetes by affecting both membrane binding and membrane permeabilization. In future research, it will be interesting to investigate the effect of more complex and physiologically relevant lipid membrane compositions.<sup>[60,61]</sup> Only recently, first TERS observations of lipid bilayers in water<sup>[62]</sup> and of cells<sup>[63]</sup> were published. Based on these advances, we anticipate that in future it will be possible to employ TERS for mapping the surface structure of hIAPP on the plasma membrane of cells in culture, although this will be a challenging experiment.

### 3. Conclusion

We have characterized the structure and amino acid residue composition of hIAPP amyloid fibrils using TERS. Our results show that TERS provides structural information with nanoscale resolution in the lateral direction. The surface of hIAPP amyloid fibrils is heterogeneous and mainly composed of unordered or  $\alpha$ -helical structure, while the core (which we probed with ATR/FT-IR) consists uniquely of  $\beta$ -sheets. Depending on the solution pH during formation, amyloid fibrils with various morphologies and structural compositions are formed. We show that TERS provides the unique opportunity to probe the influence of solution conditions such as pH on the structure of amyloid fibrils. hIAPP amyloid fibrils formed in acidic environments showed higher  $\beta$ -sheet contents and less Tyr residues at their surface than amyloid fibrils formed under neutral conditions. Phe and Cys residues are more pronounced on the surface than expected based on the hIAPP protein sequence. This is in agreement with several models of hIAPP protofilaments based on NMR measurements, showing a  $\beta$ -sheet core with Phe and Cys residues on the surface of the fibrils.<sup>[25]</sup> Using our high-statistics protocol on a large number of spectra, we showed the proof of principle of structural characterization of hIAPP amyloid fibrils formed at a lipid interface, which is more representative of the situation in vivo. The amyloid fibrils were partly covered by lipid molecules and showed mainly unordered or  $\alpha$ -helical structure at the surface. The surface structure of the fibrils was similar to that of fibrils formed under comparable assembly conditions in bulk solution, but the amino acid residues presented at the surface were partly different. We showed that TERS gives a wealth of information, on the surface molecular structure as well as on surface-exposed amino acid residues and charged groups, thus providing insights in protein folding within the fibrils. The surface of amyloids

is generally thought to play an important role in fibril toxicity and membrane damage. In future it will be interesting to apply the same technique to investigate amyloid fibrils formed from other disease-related peptides and their interactions with potential drugs or amyloids forming at the surface of cell membranes.

### 4. Experimental Section

**hIAPP Amyloid Formation:** Synthetic hIAPP (Bachem H-7905) stock solutions were prepared by dissolving hIAPP powder in MilliQ water to a concentration of  $\approx 1$  mg mL<sup>-1</sup>. The solution was filtered using a 0.2  $\mu$ m filter to remove aggregates. The peptide concentration was calculated using the absorption at 280 nm measured with a Nanodrop (Thermo Scientific) and an extinction coefficient of 1280 cm<sup>-1</sup> M<sup>-1</sup>.<sup>[22]</sup> The solution was aliquoted and stored at -80 °C until use.

For amyloid formation in bulk, hIAPP solutions were diluted in  $50 \times 10^{-3}$  M phosphate buffer at pH = 2.0 or  $5 \times 10^{-3}$  M phosphate buffer at pH = 7.8 to concentrations of  $73 \times 10^{-6}$  M. Samples were incubated in 96-well plates on a shaking plate for 6 d at RT. For TERS measurements, a drop of the fibril suspension was incubated on clean glass slides for 10 min. The samples were washed with MilliQ and dried by air.

TERS samples for fibrils formed at the lipid monolayer were prepared using the inverse Langmuir-Schaefer technique.<sup>[64]</sup> For amyloid formation at the lipid monolayer, hIAPP was diluted to a concentration of  $1 \times 10^{-6}$  M in water in a Langmuir-Blodgett trough with a surface area of 68 cm<sup>2</sup>. A cleaned glass slide was placed in the solution parallel to the surface. Drops of a  $1 \times 10^{-3}$  M solution of DPPG (Avanti Polar Lipids) in chloroform were evenly spread on the surface; in total 11  $\mu$ L DPPG was added. The sample was incubated for 17 h at room temperature (RT). No reduction of the liquid level was observed during this period. The solution was slowly removed until the glass slide went through the air-water interface. The sample was dried by air and stored under argon until the TERS measurement.

**TERS Measurements:** TERS measurements for hIAPP fibrils formed in bulk were performed on a setup comprised of an AFM (Nanowizard I, JPK, Germany) mounted on an inverted microscope (Olympus IX, Japan). Spectra were collected with a confocal spectrometer (LabRam HR, Horiba Jobin Yvon, France) with a CCD camera (Innova 300c, USA). A 60x oil immersion objective (N.A. 1.45) was used to focus the laser ( $\lambda = 530$  nm,  $P = 0.42$  mW on the sample). The acquisition time was 10 s.

For the TERS measurements for hIAPP fibrils formed at the lipid interface, a setup comprised of an AFM (Nanowizard II, JPK, Germany) mounted on an inverted Raman microscope with confocal spectrometer (SP2750A, Acton Advanced, Princeton Instruments Roper Scientific, USA) and CCD camera (Pixis 400, Princeton Instruments Roper Scientific, USA) was used. The incident laser ( $\lambda = 532$  nm,  $P = 1$  mW on sample) was focused through a 40x (N.A. 1.35) oil immersion objective on the sample. Spectra were collected with an acquisition time of 1–5 s.

TERS tips were prepared by 25 nm silver evaporation on commercial AFM noncontact tips (NSG10, NT-MDT, Russia).

**Atomic Force Microscopy:** For AFM samples, 40  $\mu$ L of the hIAPP fibril suspension was incubated on freshly cleaved mica

(15 × 15 mm) for 5 min. Samples were washed with MilliQ water and dried in air. AFM images were made in tapping mode on a Dimension 3100 scanning probe microscope (Bruker). Silicon cantilevers (TESPA, Bruker) with a spring constant of 42 N m<sup>-1</sup> were used. Images were flattened using Nanoscope 6.14 software.

**Scanning Transmission Electron Microscopy:** Fibril suspensions were diluted to peptide concentrations of 15 × 10<sup>-6</sup> M. Samples for STEM were prepared by incubation of 1 μL of the fibril suspension on a carbon coated copper grid with 300 μm mesh size (TED PELLA INC) for 5 min. Excess liquid was removed, the samples were washed with MilliQ water and dried by air. Scanning transmission electron microscopy was performed on a Verios 460 microscope (FEI) operating at 25 kV. Images were obtained in bright field.

**FT-IR Spectroscopy:** Infrared spectroscopy was carried out on a Nicolet 730 FT-IR spectrometer (Thermo Fisher Scientific Inc., Pittsburgh, PA) equipped with a liquid nitrogen cooled mercury cadmium telluride detector. The spectral resolution was 4 cm<sup>-1</sup> and for each measurement 256 spectra were averaged. The Happ-Genzel apodization function was used for the Fourier transformation. 5 μL of the respective amyloid suspension in buffer was hydrophobically attached onto the surface of a diamond attenuated total reflectance (ATR) cell (single reflection, Thermo Spectra Tech, Thermo Fisher Scientific Inc.) by drying of the suspension in air for a few minutes. Quantitative secondary structure analysis was based on the vibrational amide I band. Gaussian shaped line widths of spectral components were used for fitting as described elsewhere<sup>[65]</sup> using OriginPro 8.5.1G software.

## Supporting Information

Supporting Information is available from the Wiley Online Library or from the author.

## Acknowledgements

The authors thank A. Lof and E. Garnett (FOM Institute AMOLF) for help with STEM imaging. This work is part of the Industrial Partnership Programme (IPP) Bio(-Related) Materials (BRM) of the Stichting voor Fundamenteel Onderzoek der Materie (FOM), which is financially supported by the Nederlandse Organisatie voor Wetenschappelijk Onderzoek (NWO). The IPP BRM was cofinanced by the Top Institute Food and Nutrition and the Dutch Polymer Institute. This work is supported by NanoNextNL, a micro- and nanotechnology consortium of the Government of the Netherlands and 130 partners.

- [1] M. Stefani, C. M. Dobson, *J. Mol. Med.* **2003**, *81*, 678.
- [2] T. P. Knowles, A. W. Fitzpatrick, S. Meehan, H. R. Mott, M. Vendruscolo, C. M. Dobson, M. E. Welland, *Science* **2007**, *318*, 1900.
- [3] M. R. H. Krebs, K. R. Domike, D. Cannon, A. M. Donald, *Faraday Discuss.* **2008**, *139*, 265.
- [4] E. T. A. S. Jaikaran, A. Clark, *Biochim. Biophys. Acta, Mol. Basis Dis.* **2001**, *1537*, 179.
- [5] L. R. Volpatti, M. Vendruscolo, C. M. Dobson, T. P. J. Knowles, *ACS Nano* **2013**, *7*, 10443.
- [6] S. Zhang, M. Andreasen, J. T. Nielsen, L. Liu, E. H. Nielsen, J. Song, G. Ji, F. Sun, T. Skrydstrup, F. Besenbacher, N. C. Nielsen, D. E. Otzen, M. Dong, *Proc. Natl. Acad. Sci. U.S.A.* **2013**, *110*, 2798.
- [7] C. Goldsbury, U. Baxa, M. N. Simon, A. C. Steven, A. Engel, J. S. Wall, U. Aebi, S. A. Müller, *J. Struct. Biol.* **2011**, *173*, 1.
- [8] C. Goldsbury, K. Goldie, J. Pellaud, J. Seelig, P. Frey, S. A. Müller, J. Kistler, G. J. S. Cooper, U. Aebi, *J. Struct. Biol.* **2000**, *130*, 352.
- [9] P. Westermark, A. Andersson, G. T. Westermark, *Physiol. Rev.* **2011**, *91*, 795.
- [10] G. J. Cooper, A. C. Willis, A. Clark, R. C. Turner, R. B. Sim, K. B. Reid, *Proc. Natl. Acad. Sci. U.S.A.* **1987**, *84*, 8628.
- [11] A. Abedini, A. M. Schmidt, *FEBS Lett.* **2013**, *587*, 1119.
- [12] Y. A. Domanov, P. K. J. Kinnunen, *J. Mol. Biol.* **2008**, *376*, 42.
- [13] S. A. Jayasinghe, R. Langen, *Biochim. Biophys. Acta, Biomembr.* **2007**, *1768*, 2002.
- [14] J. Janson, R. H. Ashley, D. Harrison, S. McIntyre, P. C. Butler, *Diabetes* **1999**, *48*, 491.
- [15] M. Anguiano, R. J. Nowak, P. T. Lansbury, *Biochemistry* **2002**, *41*, 11338.
- [16] M. F. M. Engel, *Chem. Phys. Lipids* **2009**, *160*, 1.
- [17] M. F. M. Engel, L. Khemtémourian, C. C. Kleijer, H. J. D. Meeldijk, J. Jacobs, A. J. Verkleij, B. de Kruijff, J. A. Killian, J. W. M. Hoepfener, *Proc. Natl. Acad. Sci. U.S.A.* **2008**, *105*, 6033.
- [18] J. D. Green, L. Kreplak, C. Goldsbury, X. L. Blatter, M. Stolz, G. S. Cooper, A. Seelig, J. Kist-Ler, U. Aebi, *J. Mol. Biol.* **2004**, *342*, 877.
- [19] J. D. Knight, A. D. Miranker, *J. Mol. Biol.* **2004**, *341*, 1175.
- [20] J. D. Knight, J. A. Hebda, A. D. Miranker, *Biochemistry* **2006**, *45*, 9496.
- [21] L. Fu, G. Ma, E. C. Y. Yan, *J. Am. Chem. Soc.* **2010**, *132*, 5405.
- [22] M. F. M. Engel, C. C. vandenAkker, M. Schleegeer, K. P. Velikov, G. H. Koenderink, *J. Am. Chem. Soc.* **2012**, *134*, 14781.
- [23] S. A. Jayasinghe, R. Langen, *Biochemistry* **2005**, *44*, 12113.
- [24] S. B. Padrick, A. D. Miranker, *Biochemistry* **2002**, *41*, 4694.
- [25] S. Luca, W. M. Yau, R. Leapman, R. Tycko, *Biochemistry* **2007**, *46*, 13505.
- [26] J. J. W. Wiltzius, S. A. Sievers, M. R. Sawaya, D. Cascio, D. Popov, C. Riek, D. Eisenberg, *Protein Sci.* **2008**, *17*, 1467.
- [27] S. Bedrood, Y. Li, J. M. Isas, B. G. Hegde, U. Baxa, I. S. Haworth, R. Langen, *J. Biol. Chem.* **2012**, *287*, 5235.
- [28] R. Kayed, J. Bernhagen, N. Greenfield, K. Sweimeh, H. Brunner, W. Voelter, A. Kapurniotu, *J. Mol. Biol.* **1999**, *287*, 781.
- [29] A. Kapurniotu, *Biopolymers* **2001**, *60*, 438.
- [30] A. T. Petkova, R. D. Leapman, Z. Guo, W.-M. Yau, M. P. Mattson, R. Tycko, *Science* **2005**, *307*, 262.
- [31] C. C. vandenAkker, M. F. M. Engel, K. P. Velikov, M. Bonn, G. H. Koenderink, *J. Am. Chem. Soc.* **2011**, *133*, 18030.
- [32] C. Goldsbury, P. Frey, V. Olivieri, U. Aebi, S. A. Müller, *J. Mol. Biol.* **2005**, *352*, 282.
- [33] M. Stefani, *Curr. Protein Pept. Sci.* **2010**, *11*, 343.
- [34] K. F. Domke, B. Pettinger, *Chem. Phys. Chem.* **2010**, *11*, 1365.
- [35] E. Bailo, V. Deckert, *Chem. Soc. Rev.* **2008**, *37*, 921.
- [36] T. Schmid, L. Opilik, C. Blum, R. Zenobi, *Angew. Chem. Int. Ed.* **2013**, *52*, 5940.
- [37] E. A. Pozzi, M. D. Sonntag, N. Jiang, J. M. Klingsporn, M. C. Hersam, R. P. Van Duyne, *ACS Nano* **2013**, *7*, 885.
- [38] T. Ichimura, S. Fujii, P. Verma, T. Yano, Y. Inouye, S. Kawata, *Phys. Rev. Lett.* **2009**, *102*, 186101.
- [39] T. Deckert-Gaudig, V. Deckert, *Curr. Opin. Chem. Biol.* **2011**, *15*, 719.
- [40] D. Kurouski, T. Deckert-Gaudig, V. Deckert, I. K. Lednev, *J. Am. Chem. Soc.* **2012**, *134*, 13323.
- [41] T. Deckert-Gaudig, E. Kämmer, V. Deckert, *J. Biophotonics* **2012**, *5*, 215.

- [42] D. Kurouski, T. Deckert-Gaudig, V. Deckert, I. K. Lednev, *Biophys. J.* **2014**, *106*, 263.
- [43] M. Paulite, C. Blum, T. Schmid, L. Opilik, K. Eyer, G. C. Walker, R. Zenobi, *ACS Nano* **2013**, *7*, 911.
- [44] I. Amenabar, S. Poly, W. Nuansing, E. H. Hubrich, A. A. Govyadinov, F. Huth, R. Krutohovostov, L. Zhang, M. Knez, J. Heberle, A. M. Bittner, R. Hillenbrand, *Nat. Commun.* **2013**, *4*, 2890.
- [45] R. Srinivasan, E. M. Jones, K. Lui, J. Ghiso, R. E. Marchant, M. G. Zagorski, *J. Mol. Biol.* **2003**, *333*, 5.
- [46] R. P. McGlinchey, Z. P. Jiang, J. C. Lee, *Chem Bio Chem* **2014**, *15*, 1569.
- [47] L. Khemtémourian, E. Domenech, J. P. F. Doux, M. C. Koorengel, J. A. Killian, *J. Am. Chem. Soc.* **2011**, *133*, 39.
- [48] B. Bjellqvist, G. J. Hughes, C. Pasquali, N. Paquet, F. Ravier, J.-C. Sanchez, S. Frutiger, D. Hochstrasser, *Electrophoresis* **1993**, *14*, 1023.
- [49] D. Kurouski, T. Postiglione, T. Deckert-Gaudig, V. Deckert, I. K. Lednev, *Analyst* **2013**, *138*, 1665.
- [50] S. Stewart, P. M. Fredericks, *Spectrochim. Acta, Part A* **1999**, *55*, 1641.
- [51] G. Socrates, *Infrared and Raman Characteristic Group Frequencies*, 3rd ed., John Wiley & Sons, New York **2004**.
- [52] M. Paulite, C. Blum, T. Schmid, L. Opilik, K. Eyer, G. C. Walker, R. Zenobi, *ACS Nano* **2013**, *7*, 911.
- [53] R. Bohme, M. Mkandawire, U. Krause-Buchholz, P. Rosch, G. Rodel, J. Popp, V. Deckert, *Chem. Commun.* **2011**, *47*, 11453.
- [54] A. Downes, D. Salter, A. Elfick, *J. Phys. Chem. B* **2006**, *110*, 6692.
- [55] C. Blum, T. Schmid, L. Opilik, N. Metanis, S. Weidmann, R. Zenobi, *J. Phys. Chem. C* **2012**, *116*, 23061.
- [56] R. Böhme, D. Cialla, M. Richter, P. Rösch, J. Popp, V. Deckert, *J. Biophotonics* **2010**, *3*, 455.
- [57] R. Bohme, M. Richter, D. Cialla, P. Rosch, V. Deckert, J. Popp, *J. Raman Spectrosc.* **2009**, *40*, 1452.
- [58] T. Lefevre, M. Subirade, *Biopolymers* **2000**, *54*, 578.
- [59] H. Zhao, E. K. Tuominen, P. K. Kinnunen, *Biochemistry* **2004**, *43*, 10302.
- [60] P. Cao, D. P. Raleigh, *Biochemistry* **2012**, *51*, 2670.
- [61] H. Wang, P. Cao, D. P. Raleigh, *J. Mol. Biol.* **2013**, *425*, 492.
- [62] A. Nakata, T. Nomoto, T. Toyota, M. Fujinami, *Anal. Sci.* **2013**, *29*, 865.
- [63] M. Watkins-Mariani, T. Deckert-Gaudig, V. Deckert, *Anal. Bioanal. Chem.* **2014**, *406*, 27.
- [64] K. Y. C. Lee, M. M. Lipp, D. Y. Takamoto, E. Ter-Ovanesyan, J. A. Zasadzinski, A. J. Waring, *Langmuir* **1998**, *14*, 2567.
- [65] J. L. R. Arrondo, A. Muga, J. Castresana, F. M. Goni, *Prog. Biophys. Mol. Biol.* **1993**, *59*, 23.

Received: February 26, 2015  
Published online: May 7, 2015